ACS Photonics

Article

pubs.acs.org/journal/apchd5

Subdiffraction Light Concentration by J-Aggregate Nanostructures

Adriano Cacciola,[†] Claudia Triolo,[†] Omar Di Stefano,[†] Armando Genco,[‡,§] Marco Mazzeo,[§,⊥] Rosalba Saija,[†] Salvatore Patanè,[†] and Salvatore Savasta*[,†]

[†]Dipartimento di Fisica e di Scienze della Terra, Università di Messina, Viale F. Stagno d'Alcontres 31, I-98166 Messina, Italy

[‡]CBN, Center for Bio-Molecular Nanotechnologies@UNILE, Istituto Italiano di Tecnologia, via Barsanti sn, Arnesano, LE-73010 Italy

[§]Dipartimento di Matematica e Fisica "Ennio De Giorgi", Università del Salento, Via per Arnesano, 73100 Lecce, Italy

[⊥]CNR NANOTEC, Istituto di Nanotecnologia, Polo di Nanotecnologia c/o Campus Ecotekne, Via Monteroni, 73100 Lecce, Italy

Supporting Information

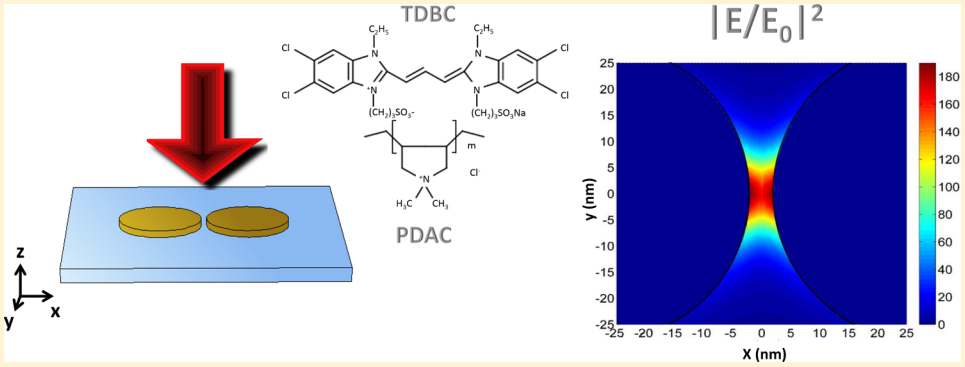

ABSTRACT: We show, by accurate scattering calculations, that nanostructures obtained from thin films of J-aggregate dyes, despite their insulating behavior, are able to concentrate the electromagnetic field at optical frequencies like metallic nanoparticles. These results promise to widely enlarge the range of plasmonic materials, thus opening new perspectives in nanophotonics. Specifically we investigate ultrathin nanodisks and nanodisk dimers that can be obtained by standard nanolithography and nanopatterning techniques. These molecular aggregates display highly attractive nonlinear optical properties, which can be exploited for the realization of ultracompact devices for switching by light on the nanoscale without the need of additional nonlinear materials.

KEYWORDS: *J-aggregates, nanophotonics, excitons, surface waves, plasmonics, light harvesting*

When light interacts with metal nanoparticles and nanostructures, it can excite collective oscillations known as localized surface plasmons (LSPs), which provide the opportunity to confine light to very small dimensions below the diffraction limit.[1−4] This high confinement can lead to a striking near-field enhancement, which can significantly enhance weak nonlinear processes[5] and enables a great variety of applications such as optical sensing,[6,7] higher efficiency solar cells,[8] nanophotonics[1,5,9] including ultracompact lasers and amplifiers,[10] and antennas transmitting and receiving light signals at the nanoscale.[4,11,12] The small mode volume of LSP resonances also increases the photonic local density of states (LDOS) close to a plasmonic nanoparticle, enabling the modification of the optical properties (decay rate and quantum efficiency) of emitters placed in its close proximity (see for example ref 13 and Supporting Information Figure S1). The interaction of quantum emitters, as quantum dots or dye molecules, with individual metallic nanostructures carries significant potential for the quantum control of light at the nanoscale.[1,14−22] As first highlighted by Takahara et al.,[23] only materials with a negative real part of the dielectric function and moderate losses are able to excite localized surface plasmons and hence to confine light to very small dimensions below the diffraction limit. These collective and confined excitations are efficiently supported, despite dissipative losses, by noble metals where the effective response of the electrons can be described by a Drude−Lorentz dielectric function whose real part is negative for frequencies below the plasma frequency.[2] Also superconductors or graphene has been proposed as a platform for surface plasmon polaritons.[24,25]

Collective oscillations of free electrons are not the only way a negative permittivity may arise. It may also occur in the high-energy tail of a strong absorption resonance. For example, it has been shown that lattice vibrations in polar dielectric materials can also originate negative dielectric permittivity in the far- or mid-infrared spectral range, which can support phonon-polaritons confined to the surface.[26,27] It has also been shown

Received: April 14, 2015
Published: June 11, 2015

DOI: 10.1021/acsphotonics.5b00197
ACS Photonics 2015, 2, 971−979

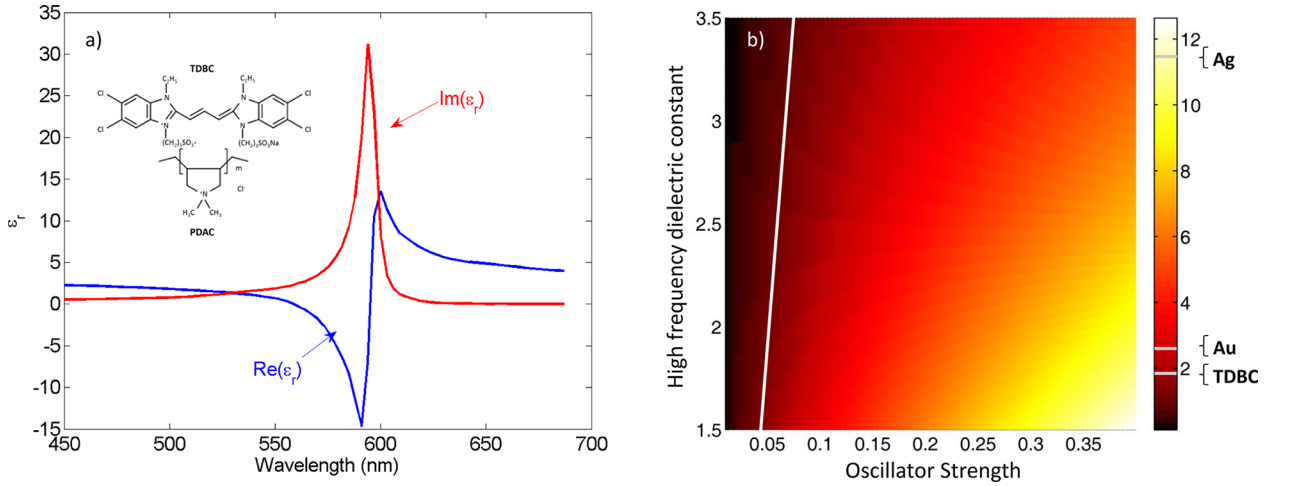

Figure 1. Plasmon-like properties in the blue-side spectral region of strong excitonic resonances. (a) Real and imaginary part of the dielectric function directly derived by the complex refractive index ($\tilde{n} = n + i\kappa$) obtained via a Kramers−Kronig regression of reflectance data[32] of layer by layer assembled TDBC/PDAC thin films. The real part of the dielectric function is negative in the blue-side region, a key feature for confining light below the diffraction limit. The inset shows the molecular structure of the polycation PDAC and of the anion TDBC, a J-aggregate-forming cyanine dye. (b) Colormap of the peak extinction efficiency $Q_{ext} = \sigma_{ext}/(\pi a^2)$ calculated in the quasistatic approximation for a 40 nm sphere in a vacuum by using the Lorentz dielectric function as a function of the normalized oscillator strength f and the high-frequency dielectric constant ε_∞ with fixed $Q_0 = 80$. The white line in the contour plot separates the region where $\varepsilon_{min} < -2$ (on the right side) and plasmon-like effects start to be expected, from the left region where $\varepsilon_{min} > -2$. This model map points out the plasmonic potentiality of excitonic resonances with high oscillator strengths. The corresponding values of Q_{ext} calculated for Ag, Au, and TDBC/PDAC nanoparticles are indicated in the color bar for reference.

that in the near-infrared and optical spectral ranges sharp excitonic resonances in organic molecules can originate spectral regions where the dielectric permittivity is negative.[28,29] The response of Lorentzian/excitonic nanoshells with an optically inactive core and embedding medium has been also studied in the quasistatic limit and compared with the properties of the Drude/plasmonic nanoshells.[30] Recently, it has been theoretically shown that a nanosphere of TDBC-doped PVA displays enhanced optical fields and subwavelength field confinement analogously to plasmonic nanoparticles.[31] At present, however, spherical nanoparticles of J-aggregates have not been realized and the synthesis of high-quality nanospheres does not seem readily achievable.

Here we propose more realistic J-aggregate nanostructures suitable for obtaining on-chip strong subwavelength light confinement. By accurate scattering calculations, we show that thin films of J-aggregate dyes[32] can be exploited for the realization of plasmon-like nanostructures working at optical frequencies. Such nanostructures can be realized after the film growth by standard nanolithography and nanopatterning techniques. The proposed structures consist of ultrathin nanodisks on a silica substrate. Moreover, we show that these molecular aggregates can also be exploited for the realization of more complex plasmon-like nanostructures to achive very high field concentration. Specifically we find that nanodisk dimers with radius a = 30 nm are able to generate near-field enhancements $|E/E_0|^2$ beyond 350. The here-proposed J-aggregate nanostructures are promising toward the realization of a low-cost plasmonic technology for the development of ultracompact photonic and optoelectronic devices. Moreover, J-aggregates display significant optical nonlinearities,[33,34] which can induce switchable localized surface resonances (LSRs) required for the realization of plasmonic devices[5] without the need to exploit the coupling with additional nonlinear optical materials.[34,35] This target has not been achieved by metallic nanoparticles owing to their intrinsically weak optical nonlinearities, which can be overcome only by coupling LSPs to nonlinear optical resonances.[34,35]

J-Aggregate self-assembled nanostructures have been realized in various forms including quasi-one-dimensional chains, single monolayers, and tubes, which could be employed as molecular plasmonic materials.[36] One limitation of these surface resonances is that they can manifest in a limited spectral region in the high-energy side of the excitonic resonance. However, because of the huge variety of organic dyes that can aggregate, it could be possible to create J-aggregate LSRs within an arbitrary part of the visible and near-IR spectrum,[37] and there is room for chemically engineering and optimizing their plasmonic behavior in order to minimize losses. Moreover J-aggregates emit light, generally with good quantum efficiencies; thus their LSRs could be exploited for the realization of efficient light-emitting nanoantennas.

These J-aggregates possess remarkable morphological and optical properties that make them suited for use in photonic and optoelectronic applications.[38−41] The broad absorption line corresponding to the single-molecule excitation is shifted to the red side of the spectrum and transforms into a collective narrow line width optical transition possessing a giant oscillator strength derived from the coherent coupling of the aggregated molecules.[42] Layer by layer growth of cyanine dye (TDBC) aggregates to form an ordered thin film has been demonstrated with a peak absorption constant of $\alpha \simeq 1 \times 10^6$ cm^{-1}, one of the highest reported for a thin film.[32] The Frenkel excitons of these highly absorptive materials have been exploited in demonstrations of strong coupling between excitons and microcavity photons,[38] room-temperature operation of exciton-optoelectronic devices,[39] strong coupling between excitons and surface plasmon-polaritons,[40] or LSP resonances.[41]

The dielectric function at frequencies around sharp excitonic resonances is usually quite well reproduced by the Lorentz model: $\varepsilon(\omega) = \varepsilon_\infty + [f\omega_0^2/(\omega_0^2 - \omega^2 - i\gamma_0\omega)]$, where ω_0 is the resonance frequency, γ_0 the width of the resonance, f the

DOI: 10.1021/acsphotonics.5b00197
ACS Photonics 2015, 2, 971−979

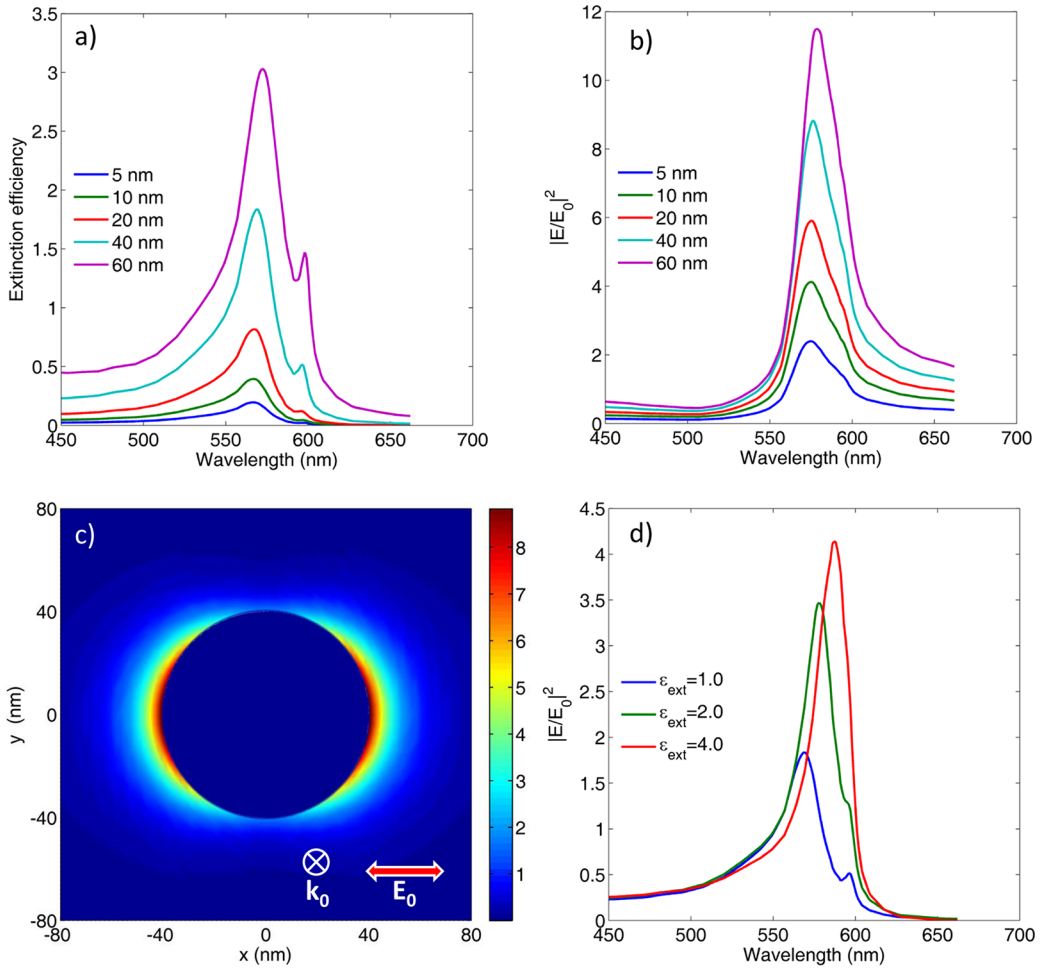

Figure 2. Scattering calculations on TDBC/PDAC nanospheres. (a) Extinction efficiency Q_{ext} for TDBC spherical nanoparticles in a vacuum of different radii a, calculated beyond the quasistatic approximation, by employing the Mie theory implemented within the T-matrix formalism. (b) Near-field enhancement spectra $|E/E_0|^2$ for the TDBC spherical nanoparticles. (c) Near-field enhancement distribution on the plane containing the polarization axis and normal to the propagation direction for a TDBC nanoparticle with a radius a = 40 nm illuminated by a plane wave at λ = 578 nm. (d) Near-field enhancement spectra as in (b) but with different dielectric constants of the external surrounding medium.

dimensionless oscillator strength, and ε_∞ the high-frequency background constant. In contrast to the Drude dielectric function, whose real part is negative for frequencies below the plasma frequency, the real part of the Lorentz dielectric function is generally positive for almost all excitonic absorption lines. It takes its minimum $\varepsilon'_{min} \simeq \varepsilon_\infty - f\omega_0/2\gamma_0$ at $\omega_{min} \simeq \omega_0 + \gamma_0/2$. However, there is no specific constraint preventing negative values. For narrow absorption lines and high oscillator strengths, the real part of the Lorentz dielectric function can acquire negative values on the high-energy side of the excitonic resonance if $f\,Q_0/2\varepsilon_\infty > 1$, where $Q_0 = \omega_0/\gamma_0$ is the quality factor of the excitonic line. The giant oscillator strength and the strong spectral narrowing of TDBC aggregates, both induced by the coherent intermolecular coupling, result in ordered thin films with a negative dielectric function in the high-energy tail of the excitonic resonance with an astonishingly low minimum value $\varepsilon_{min} \simeq -14$. Figure 1a displays the dielectric function directly derived by the real and imaginary components of the refractive index ($\tilde{n} = n + i\kappa$) obtained via a Kramers–Kronig regression of neat film reflectance data.[32] The obtained optical constants accurately reproduce both the reflectance and transmittance data for a 5 nm thick thin film and the reflectance of more complex planar optical structures containing a thin TDBC/PDAC film.[43]

The obtained TDBC/PDAC dielectric function shown in Figure 1a qualitatively resembles a Lorentz dielectric function. However, its imaginary part displays a tail in the blue part of the spectrum due to the presence of the vibrational degrees of freedom, and the Kramers–Kronig related real part is also asymmetric.

RESULTS

In order to explore the potentialities of J-aggregates as plasmonic materials, we start with the most convenient geometry for an analytical treatment: a spherical nanoparticle of radius a much smaller than the effective wavelength $\lambda/\sqrt{\varepsilon_d}$, where ε_d is the dielectric constant (assumed to be real) of the surrounding medium. Scattering calculations on more feasible J-aggregate nanostructures will be presented later. The signature of LSP effects can be easily recognized by the polarizability $\alpha_p = P/(\varepsilon_0\varepsilon_d E_0)$, defined as the ratio between the dipole moment P induced in the nanoparticle by an incoming wave and the amplitude of the incident displacement field E_0. In the quasistatic approximation, for a spherical nanoparticle, $\alpha_p = 4\pi a^3(\varepsilon(\omega) - \varepsilon_d)/(\varepsilon(\omega) + 2\varepsilon_d)$. The nanoparticle polarizability displays a dipole resonance when $\varepsilon'(\omega) = -2\varepsilon_d$, known as the Frölich condition. The optical theorem provides a direct link

DOI: 10.1021/acsphotonics.5b00197
ACS Photonics 2015, 2, 971–979

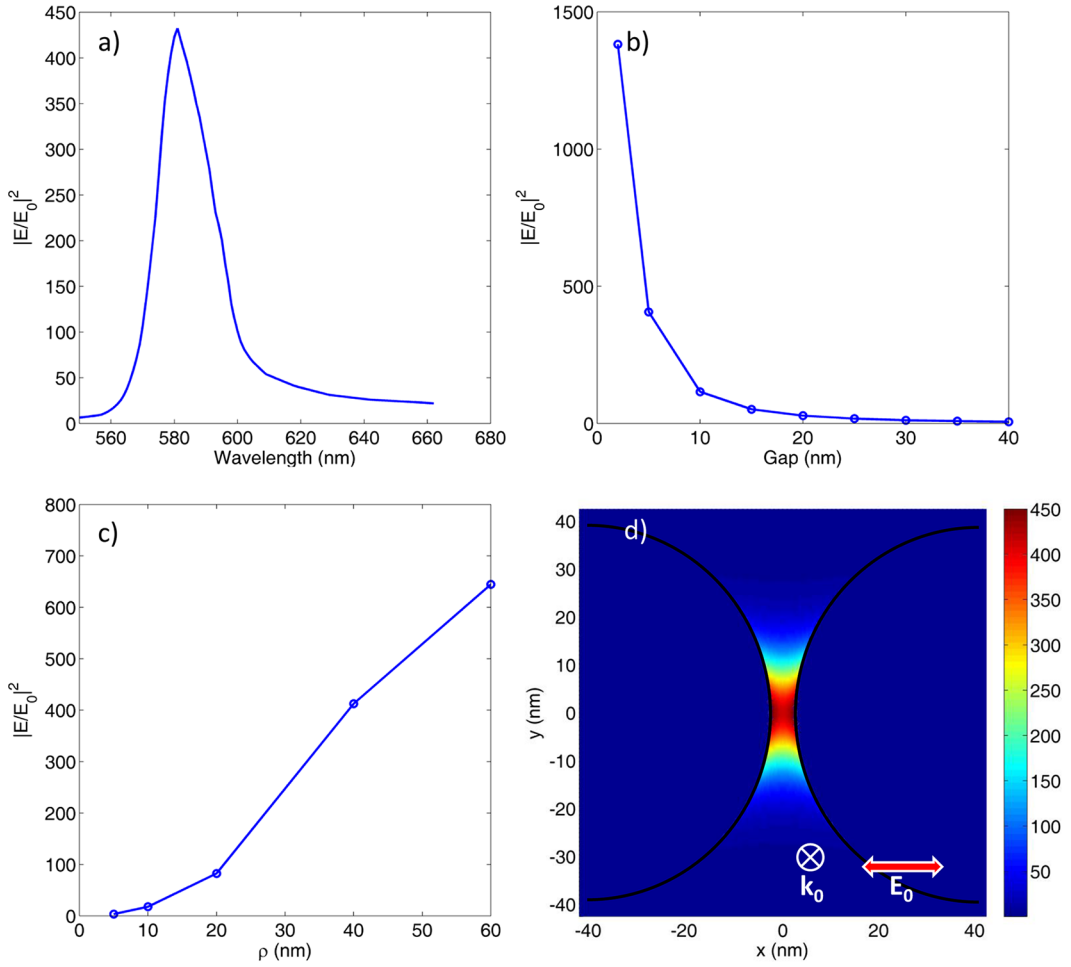

Figure 3. Scattering calculations for a dimer of two nanospheres in vacuum illuminated by longitudinally polarized plane waves. (a) Near-field enhancement spectrum calculated at the center of a 5 nm gap between two nanospheres (radius a = 40 nm). (b) Peak field enhancement at the center of the gap as a function of the gap (a = 40 nm). (c) Peak field enhancement at the center of a 5 nm gap as a function of the nanoparticle radius. (d) Near-field enhancement distribution around the nanostructure on the plane $z = h/2$ for h = 5 nm calculated for an incident plane wave at λ = 581 nm.

between the polarizability and the extinction cross section $\sigma_{ext} = \varepsilon_d^{1/2} k_0 \, \mathrm{Im}\{\alpha_p\}$, where $k_0 = 2\pi/\lambda$. This resonance also produces a resonant enhancement of the dipolar field and of the optical LDOS around the nanoparticle. Many of the attractive plasmonic applications of metal nanoparticles and nanostructures rely on this field enhancement at the plasmon resonance.[1,3,4,6,8,9,14] In Figure 1b a model map points out the plasmonic potentiality of strong excitonic resonances. The figure displays the peak extinction efficiency $Q_{ext} = \sigma_{ext}/(\pi a^2)$ for a 40 nm sphere calculated within the quasistatic approximation by using the Lorentz dielectric function versus the normalized oscillator strength f and the high-frequency dielectric constant ε_∞ with fixed Q_0 = 80.

Figure 2a displays the extinction efficiency Q_{ext} for TDBC spherical nanoparticles of different radii a, calculated beyond the quasistatic approximation, by employing the Mie theory implemented within the T-matrix formalism[20,44] (see also the Methods section). It is remarkable that a Q_{ext} slightly larger than 3 is observed for a nanoparticle with a radius of 60 nm. This means that the interception area that the spherical particle presents to the incident radiation is about 3 times larger than its actual size. Such extinction efficiency is lower than that for a gold nanoparticle with the same radius (see also the color bar in Figure 1b), but it is significantly larger than the efficiency of dielectric particles with positive dielectric functions. It is worth noticing that the extinction spectra display peaks at the wavelength corresponding to the LSR, which is significantly blue-shifted with respect to the excitonic absorption maximum (compare Figure 1 and Figure 2a). Figure 2a also displays a significantly smaller peak corresponding to the excitonic resonance. Figure 2b shows the calculated near-field enhancement spectra $|E/E_0|^2$ for the TDBC nanoparticles. The field has been calculated at a distance d = 1 nm from the surface of the nanoparticle at an angle between the incident electric field and the position vector (with the origin at the nanoparticle center) θ = 0. A significant plasmon-like near-field enhancement (beyond 1 order of magnitude for the a = 60 nm nanoparticle) can be observed. Such enhancement is about one-half of the enhancement induced by a gold nanoparticle of the same size. The wavelength where the maximum enhancement occurs is red-shifted with respect to the corresponding extinction-spectrum peak, which is a typical plasmonic feature.[45] Figure 2c shows the near-field enhancement distribution on the plane containing the polarization axis and normal to the propagation direction for a TDBC nanoparticle with a radius a = 40 nm. Calculations have been performed considering an incident plane wave at λ = 578 nm. The influence of the dielectric environment on the LSR resonance is shown in Figure 2d. A

DOI: 10.1021/acsphotonics.5b00197
ACS Photonics 2015, 2, 971−979

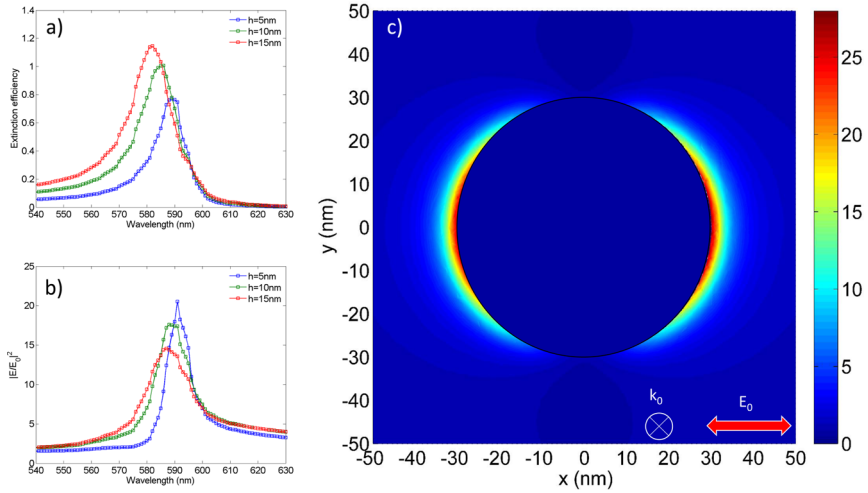

Figure 4. Scattering calculations on single nanodisks. (a) Extinction efficiency Q_{ext} spectra for three single nanodisks of radius a = 30 nm and heights h = 5, 10, and 15 nm, calculated under normal illumination. (b) Near-field enhancement calculated at $z = h/2$ and at a distance d = 1 nm from the disk lateral surface along the polarization direction (θ = 0). (c) Near-field enhancement distribution on the plane $z = h/2$ and normal to the propagation direction for the TDBC nanodisk with h = 5 nm, under plane wave illumination at λ = 591 nm.

shift of the resonance due to the modification of the Frölich condition can be observed. By confining light using LSPs, it is possible to significantly alter the photonic LDOS, thus enabling a remarkable enhancement of the spontaneous emission rate of emitters placed in the near field of a metallic nanoparticle. For an emitter oriented toward a 40 nm TDBC nanoparticle center, located at a distance d = 5 nm with a transition wavelength λ_0 = 578 nm, we find a spontaneous emission enhancement $\Gamma/\Gamma_0 \simeq$ 10 (Supporting Information Figure SI1).

When two or more plasmon-resonant nanoparticles are closely spaced, LSPs of individual particles interact, giving rise to a strong optical field enhancement in the gap regions between the particles.[46−48] As a further signature of the plasmonic behavior of TDBC nanoparticles, we show that such a strong enhancement can be observed with J-aggregate TDBC dimers. The near-field enhancement spectrum $|E/E_0|^2$ calculated at the center of the gap between two nanospheres with a = 40 nm is reported in Figure 3a. All the presented calculations for dimers have been obtained considering a longitudinally polarized incident field (along the dimer axis). The peak field enhancement at the center of the gap between two TDBC spherical nanoparticles (a = 40 nm) as a function of the gap is reported in Figure 3b. Figure 3c shows the peak field enhancement at the center of a 5 nm gap as a function of the nanoparticle radius. The near-field enhancement distribution on the plane containing the dimer axis and orthogonal to the propagation direction is displayed in Figure 3d. At present, spherical nanoparticles of J-aggregates have not been realized, and we are not aware of any present growing technique. Moreover, the dielectric function here considered has been derived by means of optical measurements on an ordered TDBC thin film grown layer by layer on a substrate.

We thus study more feasible J-aggregate nanostructures, showing a plasmon-like behavior analogous to the above-described nanospheres. Such nanostructures can be realized after the film growth by standard nanolitography and nanopatterning techniques.[49] The proposed structures consist of ultrathin nanodisks and nanodisk dimers grown on a silica substrate. Scattering calculations have been performed by the finite element method (see Methods). Figure 4a displays the extinction efficiency Q_{ext} spectra for three single nanodisks of radius a = 30 nm and heights h = 5, 10, and 15 nm, calculated under normal illumination. Increasing the thickness h, a blue-shift of the LSR is observed. This blue-shift at increasing ratios h/a is a typical plasmonic feature reported for metal nanodisks.[50] The small shoulder on the red side of the peak is a signature of the exciton absorption peak at about λ = 595 nm, corresponding to the wavelength where the imaginary part of the TDBC/PDAC dielectric function is maximum (see Figure 1a). The near-field enhancement $|E/E_0|^2$ calculated at an angle between the incident electric field and the position vector (with the origin at the nanodisk's center) θ = 0, at $z = h/2$, and at a distance d = 1 nm from the disk lateral surface, is shown in Figure 4b. Figure 4c displays the near-field enhancement distribution on the plane containing the polarization axis and normal to the propagation direction for the TDBC nanodisk with h = 5 nm. Calculations have been performed considering an incident plane wave at the near-field enhancement peak in Figure 4b. A strong field enhancement beyond 25 is observed. These results clearly show that realistic J-aggregate nanostructures are able to support LSP-like resonances. For comparison, scattering calculations for gold nanodisks have been included in the Supporting Information (Figure SI2).

It is worth observing that the dielectric function used for all the presented calculations has been obtained from optical data fitted by an isotropic model; thus any optical anisotropy effect is neglected. With J-aggregates having an intrinsically anisotropic structure,[42,51] anisotropy of the dielectric response can be expected in thin films as well. To our knowledge there are no specific data on TDBC films; however recently, by using spectroscopic ellipsometry and polarized IR spectroscopy, a strongly anisotropic behavior of thiacarbocyanine dye aggregate films was revealed.[52] It was quantified by means of two dielectric functions: one for the xy plane parallel to the film and the other for the z direction perpendicular to it. These data do not show any optical anisotropy for polarizations along the xy plane. In the Supporting Information (Figure SI3) we show optical absorbance measurements at normal incidence for two different orthogonal linear polarizations. The data confirm the absence of optical anisotropy on the xy plane. All the calculations on nanodisks have been performed by considering input light at normal incidence and hence polarized along the

DOI: 10.1021/acsphotonics.5b00197
ACS Photonics 2015, 2, 971−979

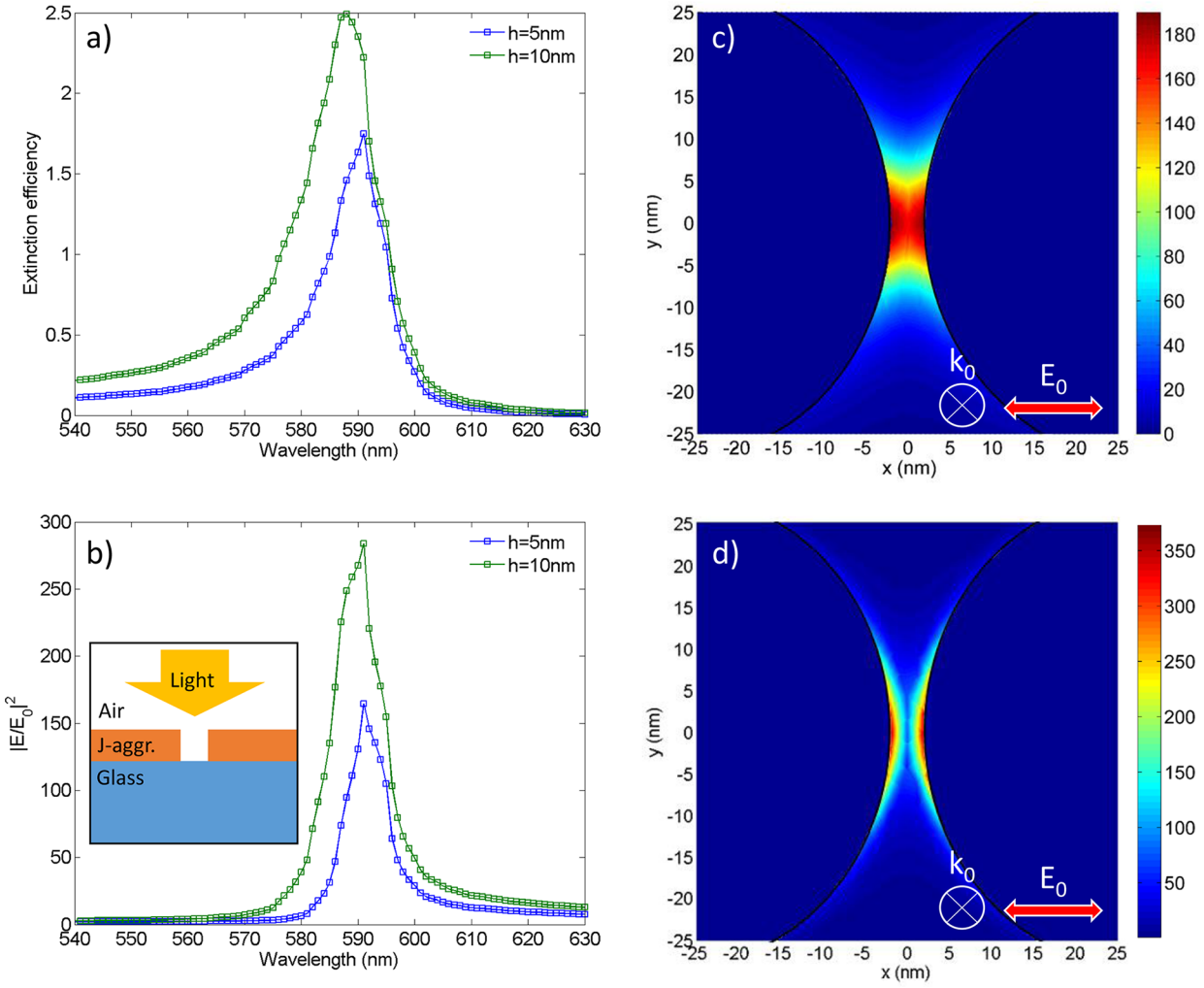

Figure 5. Scattering calculations under plane wave illumination with normal incidence and longitudinal polarization (along the dimer axis) on TDBC/PDAC nanodisk dimers on a glass substrate. The two disks have a radius a = 30 nm and are separated by a gap of 4 nm. (a) Extinction efficiency for dimers of two different heights h. (b) Near-field enhancement spectra calculated at the gap center and at $z = h/2$. (c) Near-field enhancement distribution around the nanostructure on the plane $z = h/2$ for h = 5 nm and λ = 591 nm. (d) Near-field distribution calculated on the substrate surface z = 0 for h = 5 nm and λ = 591 nm.

xy plane. In this case the near field generated by the nanodisk along the *z* axis is very small (beyond 1 order of magnitude), and thus the presence of a different dielectric function along the *z* axis does not affect significantly the obtained results. The lack of optical anisotropy in the *xy* thin film response may be due to the local disorder during the growth process, as evidenced in AFM images in ref 32. We also observe that, from available AFM images (see, for example, ref 32), it is possible to infer some degree of local order in the 100 nm range. Hence it is possible that TDBC nanodisks (or more generally nanostructures) display some degree of optical anisotropy on the *xy* plane, depending on the specific arrangement of the monomers. In this case the dielectric function that we used for all the calculations can be interpreted as an average quantity. For example for a brickwork-type arrangement of the monomers in the aggregates, a larger dipole moment can be expected along the head−tail direction of the aggregates. For the nanodisks here investigated, we would expect an increase of the near-field enhancement for input light polarized along the head−tail direction and a corresponding decrease along the orthogonal direction. Another interesting issue is the possible dependence of the dielectric function on the size of the nanostructures. As the sharp peak in the dielectric function and the corresponding negative permittivity arise from the interaction of the dye molecules, the dielectric function might strongly depend on the size of the nanostructures. According to accurate theoretical calculations including both the electronic and vibrational degrees of freedom, a chain with 15 monomers fully reproduces the observed shifted and sharp absorption peaks of J-aggregates.[53] This theoretical analysis is confirmed by femtosecond nonlinear optical experiments on TDBC J-aggregates, showing that the exciton delocalization length at room temperature corresponds to 16 molecules.[54] As a consequence, nanostrutures with linear dimensions beyond 30 nm should display the desired optical properties.

Scattering calculations on nanodisk dimers are shown in Figure 5. The two disks have a radius a = 30 nm and are separated by a gap of 4 nm. We consider dimers of two different heights h = 5 and 10 nm. The extinction efficiency and near-field enhancement spectra are shown in Figure 5a and b under plane wave illumination with normal incidence and longitudinal polarization (along the dimer axis). The enhancement spectra have been calculated at the gap center and $z = h/2$. The near-field enhancement distribution around the

DOI: 10.1021/acsphotonics.5b00197
ACS Photonics 2015, 2, 971−979

nanostructure on the plane $z = h/2$ under the above-described conditions is displayed in Figure 5c. Figure 5d shows the resulting field distribution calculated on the substrate surface ($z = 0$). A further concentration of the field around the opposite disk's surface can be observed. Analogous calculations based on an excitonic resonance providing a dielectric function with positive real part[55] display a negligible near-field enhancement (Supporting Information Figure SI4).

CONCLUSIONS

The presented results demonstrate that J-aggregate nanostructures display LSRs able to confine light below the diffraction limit, resulting in a strong near-field enhancement comparable to that induced by gold nanoparticles. These results, in view also of the huge variety of organic dyes that can aggregate and their chemical flexibility, hold the promise to greatly enlarge the availability of new plasmonic materials with different properties with respect to noble metals. For example J-aggregates display attractive nonlinear optical properties, which could be exploited for the realization of switchable LSRs for nanophotonic devices. Specifically, it has been shown that an ultrafast optical pump is able to significantly affect the dielectric function of J-aggregates;[5,34,35,51] hence we expect light-controlled modifications of the LSRs, very sensitive to the real part of the dielectric function, which can be exploited for the realization of ultracompact all-optical switches. Since analogous molecular aggregates can be found in nature,[56] acting as antennas in photosynthetic complexes, the results here presented open the intriguing question if photosynthetic organisms[57] exploit LSRs to improve light-harvesting efficiency.[58,59] At the same time J-aggregate nanoantennas could represent a low-cost solution for improving photovoltaic devices and for the realization of efficient artificial photosynthetic light-harvesting antennas.[60]

METHODS

Scattering calculations on spherical nanoparticles and dimers have been performed within the transition-matrix method, initially introduced by Waterman[61] as a general technique for computing the EM scattering based on the Huygens principle. In the last decades this method has been significantly improved by expanding the incident, the internal, and the scattered electromagnetic fields in vector spherical harmonics (VSH).[44] Thanks to the linearity of Maxwell's equations and boundary conditions, when the scatterers, either single or aggregate, are constituted by spherical monomers, the expansion of the electromagnetic fields in terms of VSH allows the analytical relation of the multipolar amplitude of incident field to those of the scattered field by means of the T-matrix. The transition matrix contains all the information on the microphysical properties of the scatterer, being independent from the state of polarization of incidence field and from the incident and observation direction. The elements of the T-matrix define analytically in the far field the optical cross section and in the near-field zone the intensity distribution of the total and scattered field. From a computational point of view, the numerical calculation of the transition matrix requires the inversion of a matrix whose order is, in principle, infinite. However, it is possible to truncate the multipole expansion of the fields, which determine the size of the array, in order to ensure the numerical stability of the results.

The finite element method (FEM) is a differential equation method that computes the scattered time-harmonic electromagnetic field by solving numerically the vector Helmholtz equation subject to boundary conditions at the particle surface. Due to the discretization process (mesh construction) of the domains in smaller parts, this technique is suitable to describe systems with complex geometry. The structure, placed on a glass substrate, is embedded in a 3D finite computational domain that is discretized into many small-volume tetrahedral cells. In the far-field zone, at the outer boundary of the finite computational domain, approximate absorbing boundary conditions are imposed. In this way it is possible both to suppress wave reflections back into the domain and to allow the propagation of the numerical outgoing waves as if the domain were infinite.[62] In the near-field zone, for the 3D tetrahedral elements, we choose an extremely fine size (up to 0.1 nm) to better describe the rapid changes in the electromagnetic field. By solving 3D Helmholtz equations together with the boundary conditions in each element of the mesh, we can reconstruct the optical behavior of the system, the near-field enhancement distribution around the nanostructures (see Figures 4b, 5c,d) and the extinction spectra in the far field. Scattering calculations were validated by comparing the results with the simulation of the same spherical nanoparticles and dimers studied above with the Mie theory.

ASSOCIATED CONTENT

Supporting Information

Spontaneous emission enhancement of a TDBC nanosphere; scattering calculations based on an excitonic resonance providing a dielectric function with positive real part for a dimer; scattering calculations for a gold nanodisk. The Supporting Information is available free of charge on the ACS Publications website at DOI: 10.1021/acsphotonics.5b00197.

AUTHOR INFORMATION

Corresponding Author

*E-mail: ssavasta@unime.it.

Notes

The authors declare no competing financial interest.

ACKNOWLEDGMENTS

The authors acknowledge financial support from the MPNS COST Action MP1403 Nanoscale Quantum Optics. The authors also thank L. Monsù Scolaro for providing the data on the dielectric function in the Supporting Information and for useful discussions.

REFERENCES

(1) Maier, S. A.; Brongersma, M. L.; Kik, P. G.; Meltzer, S.; Requicha, A. A.; Atwater, H. A. Plasmonics - a route to nanoscale optical devices. *Adv. Mater.* **2001**, *13*, 1501−1505.

(2) Maier, S. A. *Plasmonics: Fundamentals and Applications*; Springer Science & Business Media, 2007.

(3) Gramotnev, D. K.; Bozhevolnyi, S. I. Plasmonics beyond the diffraction limit. *Nat. Photonics* **2010**, *4*, 83−91.

(4) Schuller, J. A.; Barnard, E. S.; Cai, W.; Jun, Y. C.; White, J. S.; Brongersma, M. L. Plasmonics for extreme light concentration and manipulation. *Nat. Mater.* **2010**, *9*, 193−204.

(5) Kauranen, M.; Zayats, A. V. Nonlinear plasmonics. *Nat. Photonics* **2012**, *6*, 737−748.

(6) Anker, J. N.; Hall, W. P.; Lyandres, O.; Shah, N. C.; Zhao, J.; Van Duyne, R. P. Biosensing with plasmonic nanosensors. *Nat. Mater.* **2008**, *7*, 442−453.

DOI: 10.1021/acsphotonics.5b00197
ACS Photonics 2015, 2, 971−979

(7) Stewart, M. E.; Anderton, C. R.; Thompson, L. B.; Maria, J.; Gray, S. K.; Rogers, J. A.; Nuzzo, R. G. Nanostructured plasmonic sensors. *Chem. Rev.* **2008**, *108*, 494−521.
(8) Atwater, H. A.; Polman, A. Plasmonics for improved photovoltaic devices. *Nat. Mater.* **2010**, *9*, 205−213.
(9) Willets, K. A.; Van Duyne, R. P. Localized surface plasmon resonance spectroscopy and sensing. *Annu. Rev. Phys. Chem.* **2007**, *58*, 267−297.
(10) Noginov, M.; Zhu, G.; Belgrave, A.; Bakker, R.; Shalaev, V.; Narimanov, E.; Stout, S.; Herz, E.; Suteewong, T.; Wiesner, U. Demonstration of a spaser-based nanolaser. *Nature* **2009**, *460*, 1110−1112.
(11) Schnell, M.; Garcia-Etxarri, A.; Huber, A.; Crozier, K.; Aizpurua, J.; Hillenbrand, R. Controlling the near-field oscillations of loaded plasmonic nanoantennas. *Nat. Photonics* **2009**, *3*, 287−291.
(12) Aouani, H.; Mahboub, O.; Devaux, E.; Rigneault, H.; Ebbesen, T. W.; Wenger, J. Plasmonic antennas for directional sorting of fluorescence emission. *Nano Lett.* **2011**, *11*, 2400−2406.
(13) Russell, K. J.; Liu, T.-L.; Cui, S.; Hu, E. L. Large spontaneous emission enhancement in plasmonic nanocavities. *Nat. Photonics* **2012**, *6*, 459−462.
(14) Ozbay, E. Plasmonics: merging photonics and electronics at nanoscale dimensions. *Science* **2006**, *311*, 189−193.
(15) Chang, D. E.; Sørensen, A. S.; Demler, E. A.; Lukin, M. D. A single-photon transistor using nanoscale surface plasmons. *Nat. Phys.* **2007**, *3*, 807−812.
(16) Ridolfo, A.; Di Stefano, O.; Fina, N.; Saija, R.; Savasta, S. Quantum plasmonics with quantum dot-metal nanoparticle molecules: influence of the Fano effect on photon statistics. *Phys. Rev. Lett.* **2010**, *105*, 263601.
(17) Savasta, S.; Saija, R.; Ridolfo, A.; di Stefano, O.; Denti, P.; Borghese, F. Nanopolaritons: vacuum Rabi splitting with a single quantum dot in the center of a dimer nanoantenna. *ACS Nano* **2010**, *4*, 6369−6376.
(18) Zengin, G.; Johansson, G.; Johansson, P.; Antosiewicz, T. J.; Käll, M.; Shegai, T. Approaching the strong coupling limit in single plasmonic nanorods interacting with J-aggregates. *Sci. Rep.* **2013**, *3*, 3074.
(19) Tame, M.; McEnery, K.; Özdemir, Ş.; Lee, J.; Maier, S.; Kim, M. Quantum plasmonics. *Nat. Phys.* **2013**, *9*, 329−340.
(20) Cacciola, A.; Di Stefano, O.; Stassi, R.; Saija, R.; Savasta, S. Ultrastrong Coupling of Plasmons and Excitons in a Nanoshell. *ACS Nano* **2014**, *8*, 11483−11492.
(21) Antosiewicz, T. J.; Apell, S. P.; Shegai, T. Plasmon-exciton interactions in a core-shell geometry: from enhanced absorption to strong coupling. *ACS Photonics* **2014**, *1*, 454−463.
(22) Zengin, G.; Wersäll, M.; Nilsson, S.; Antosiewicz, T. J.; Käll, M.; Shegai, T. Realizing strong light-matter interactions between single nanoparticle plasmons and molecular excitons at ambient conditions. *Phys. Rev. Lett.* **2015**, *114*, 157401.
(23) Takahara, J.; Yamagishi, S.; Taki, H.; Morimoto, A.; Kobayashi, T. Guiding of a one-dimensional optical beam with nanometer diameter. *Opt. Lett.* **1997**, *22*, 475−477.
(24) Tassin, P.; Koschny, T.; Kafesaki, M.; Soukoulis, C. M. A comparison of graphene, superconductors and metals as conductors for metamaterials and plasmonics. *Nat. Photonics* **2012**, *6*, 259−264.
(25) Woessner, A.; Lundeberg, M. B.; Gao, Y.; Principi, A.; Alonso-González, P.; Carrega, M.; Watanabe, K.; Taniguchi, T.; Vignale, G.; Polini, M.; Hone, J.; Hillenbrand, R.; Koppens, F. H. L. Highly confined low-loss plasmons in graphene-boron nitride heterostructures. *Nat. Mater.* **2014**, *14*, 421−425.
(26) Shchegrov, A. V.; Joulain, K.; Carminati, R.; Greffet, J.-J. Near-field spectral effects due to electromagnetic surface excitations. *Phys. Rev. Lett.* **2000**, *85*, 1548.
(27) Ocelic, N.; Hillenbrand, R. Subwavelength-scale tailoring of surface phonon polaritons by focused ion-beam implantation. *Nat. Mater.* **2004**, *3*, 606−609.
(28) Philpott, M.; Brillante, A.; Pockrand, I.; Swalen, J. A new optical phenomenon: exciton surface polaritons at room temperature. *Mol. Cryst. Liq. Cryst.* **1979**, *50*, 139−162.
(29) Gu, L.; Livenere, J.; Zhu, G.; Narimanov, E. E.; Noginov, M. Quest for organic plasmonics. *Appl. Phys. Lett.* **2013**, *103*, 021104.
(30) Gülen, D. Optical response of Lorentzian nanoshells in the quasistatic limit. *J. Phys. Chem. B* **2013**, *117*, 11220−11228.
(31) Gentile, M. J.; Núñez-Sánchez, S.; Barnes, W. Optical field-enhancement and subwavelength field-confinement using excitonic nanostructures. *Nano Lett.* **2014**, *14*, 2339−2344.
(32) Bradley, M. S.; Tischler, J. R.; Bulović, V. Layer-by-layer J-aggregate thin films with a peak absorption constant of 106 cm^{-1}. *Adv. Mater.* **2005**, *17*, 1881−1886.
(33) Minoshima, K.; Taiji, M.; Misawa, K.; Kobayashi, T. Femtosecond nonlinear optical dynamics of excitons in J-aggregates. *Chem. Phys. Lett.* **1994**, *218*, 67−72.
(34) Vasa, P.; Wang, W.; Pomraenke, R.; Lammers, M.; Maiuri, M.; Manzoni, C.; Cerullo, G.; Lienau, C. Real-time observation of ultrafast Rabi oscillations between excitons and plasmons in metal nanostructures with J-aggregates. *Nat. Photonics* **2013**, *7*, 128−132.
(35) Fofang, N. T.; Grady, N. K.; Fan, Z.; Govorov, A. O.; Halas, N. J. Plexciton dynamics: exciton−plasmon coupling in a J-aggregate−Au nanoshell complex provides a mechanism for nonlinearity. *Nano Lett.* **2011**, *11*, 1556−1560.
(36) Saikin, S. K.; Eisfeld, A.; Valleau, S.; Aspuru-Guzik, A. Photonics meets excitonics: natural and artificial molecular aggregates. *Nanophotonics* **2013**, *2*, 21−38.
(37) Walker, B. J.; Dorn, A.; Bulovic, V.; Bawendi, M. G. Color-selective photocurrent enhancement in coupled J-aggregate/nanowires formed in solution. *Nano Lett.* **2011**, *11*, 2655−2659.
(38) Lidzey, D. G.; Bradley, D.; Skolnick, M.; Virgili, T.; Walker, S.; Whittaker, D. Strong exciton-photon coupling in an organic semiconductor microcavity. *Nature* **1998**, *395*, 53−55.
(39) Tischler, J. R.; Bradley, M. S.; Bulović, V.; Song, J. H.; Nurmikko, A. Strong coupling in a microcavity LED. *Phys. Rev. Lett.* **2005**, *95*, 036401.
(40) Bellessa, J.; Bonnand, C.; Plenet, J.; Mugnier, J. Strong coupling between surface plasmons and excitons in an organic semiconductor. *Phys. Rev. Lett.* **2004**, *93*, 036404.
(41) Schlather, A. E.; Large, N.; Urban, A. S.; Nordlander, P.; Halas, N. J. Near-field mediated plexcitonic coupling and giant Rabi splitting in individual metallic dimers. *Nano Lett.* **2013**, *13*, 3281−3286.
(42) Würthner, F.; Kaiser, T. E.; Saha-Möller, C. R. J-Aggregates: from serendipitous discovery to supramolecular engineering of functional dye materials. *Angew. Chem., Int. Ed.* **2011**, *50*, 3376−3410.
(43) Tischler, J. R.; Bradley, M. S.; Bulović, V. Critically coupled resonators in vertical geometry using a planar mirror and a 5 nm thick absorbing film. *Opt. Lett.* **2006**, *31*, 2045−2047.
(44) Borghese, F.; Denti, P.; Saija, R. *Scattering from Model Nonspherical Particles: Theory and Applications to Environmental Physics*; Springer Science & Business Media, 2007.
(45) Zuloaga, J.; Nordlander, P. On the energy shift between near-field and far-field peak intensities in localized plasmon systems. *Nano Lett.* **2011**, *11*, 1280−1283.
(46) Nordlander, P.; Oubre, C.; Prodan, E.; Li, K.; Stockman, M. Plasmon hybridization in nanoparticle dimers. *Nano Lett.* **2004**, *4*, 899−903.
(47) Talley, C. E.; Jackson, J. B.; Oubre, C.; Grady, N. K.; Hollars, C. W.; Lane, S. M.; Huser, T. R.; Nordlander, P.; Halas, N. J. Surface-enhanced Raman scattering from individual Au nanoparticles and nanoparticle dimer substrates. *Nano Lett.* **2005**, *5*, 1569−1574.
(48) Halas, N. J.; Lal, S.; Chang, W.-S.; Link, S.; Nordlander, P. Plasmons in strongly coupled metallic nanostructures. *Chem. Rev.* **2011**, *111*, 3913−3961.
(49) Menard, E.; Meitl, M. A.; Sun, Y.; Park, J.-U.; Shir, D. J.-L.; Nam, Y.-S.; Jeon, S.; Rogers, J. A. Micro- and nanopatterning techniques for organic electronic and optoelectronic systems. *Chem. Rev.* **2007**, *107*, 1117−1160.

DOI: 10.1021/acsphotonics.5b00197
ACS Photonics 2015, 2, 971−979

(50) Zoric, I.; Zach, M.; Kasemo, B.; Langhammer, C. Gold, platinum, and aluminum nanodisk plasmons: material independence, subradiance, and damping mechanisms. *ACS Nano* **2011**, *5*, 2535−2546.
(51) Kobayashi, T. *J-Aggregates*; World Scientific, 1996.
(52) Roodenko, K.; Nguyen, H.; Caillard, L.; Radja, A.; Thissen, P.; Gordon, J.; Gartstein, Y. N.; Malko, A.; Chabal, Y. Anisotropic optical properties of thin-film thiacarbocyanine dye aggregates. *J. Phys. Chem. C* **2013**, *117*, 20186−20192.
(53) Roden, J.; Eisfeld, A.; Wolff, W.; Strunz, W. T. Influence of complex exciton-phonon coupling on optical absorption and energy transfer of quantum aggregates. *Phys. Rev. Lett.* **2009**, *103*, 058301.
(54) van Burgel, M.; Wiersma, D. A.; Duppen, K. The dynamics of one-dimensional excitons in liquids. *J. Chem. Phys.* **1995**, *102*, 20−33.
(55) Castriciano, M. A.; Romeo, A.; Villari, V.; Micali, N.; Scolaro, L. M. Structural rearrangements in 5,10,15,20-tetrakis (4-sulfonatophenyl) porphyrin J-aggregates under strongly acidic conditions. *J. Phys. Chem. B* **2003**, *107*, 8765−8771.
(56) Coles, D. M.; Yang, Y.; Wang, Y.; Grant, R. T.; Taylor, R. A.; Saikin, S. K.; Aspuru-Guzik, A.; Lidzey, D. G.; Tang, J. K.-H.; Smith, J. M. Strong coupling between chlorosomes of photosynthetic bacteria and a confined optical cavity mode. *Nat. Commun.* **2014**, *5*, 5561.
(57) McDermott, G.; Prince, S.; Freer, A.; Hawthornthwaite-Lawless, A.; Papiz, M.; Cogdell, R.; Isaacs, N. Crystal structure of an integral membrane light-harvesting complex from photosynthetic bacteria. *Nature* **1995**, *374*, 517−521.
(58) Engel, G. S.; Calhoun, T. R.; Read, E. L.; Ahn, T.-K.; Mančal, T.; Cheng, Y.-C.; Blankenship, R. E.; Fleming, G. R. Evidence for wavelike energy transfer through quantum coherence in photosynthetic systems. *Nature* **2007**, *446*, 782−786.
(59) Collini, E.; Wong, C. Y.; Wilk, K. E.; Curmi, P. M.; Brumer, P.; Scholes, G. D. Coherently wired light-harvesting in photosynthetic marine algae at ambient temperature. *Nature* **2010**, *463*, 644−647.
(60) Kodis, G.; Liddell, P. A.; de la Garza, L.; Clausen, P. C.; Lindsey, J. S.; Moore, A. L.; Moore, T. A.; Gust, D. Efficient energy transfer and electron transfer in an artificial photosynthetic antenna-reaction center complex. *J. Phys. Chem. A* **2002**, *106*, 2036−2048.
(61) Waterman, P. Matrix formulation of electromagnetic scattering. *Proc. IEEE* **1965**, *53*, 805−812.
(62) Mittra, R.; Ramahi, O. Absorbing boundary conditions for the direct solution of partial differential equations arising in electromagnetic scattering problems. *Prog. Electromagn. Res.* **1990**, *2*, 133−173.

DOI: 10.1021/acsphotonics.5b00197
ACS Photonics 2015, 2, 971−979